© 2019. Published by The Company of Biologists Ltd | Journal of Experimental Biology (2019) 222, jeb205963. doi:10.1242/jeb.205963

RESEARCH ARTICLE

Streak formation in flow over biomimetic fish scale arrays

Muthukumar Muthuramalingam[1,*], Leo S. Villemin[1,2] and Christoph Bruecker[1]

ABSTRACT

The surface topology of the scale pattern from the European sea bass (*Dicentrarchus labrax*) was measured using a digital microscope and geometrically reconstructed using computer assisted design modelling. Numerical flow simulations and experiments with a physical model of the surface pattern in a flow channel mimic the flow over the fish surface with a laminar boundary layer. The scale array produces regular rows of alternating, streamwise low-speed and high-speed streaks inside the boundary layer close to the surface, with maximum velocity difference of approximately 9%. Low velocity streaks are formed in the central region of the scales whereas the high velocity streaks originated in the overlapping region between the scales. Thus, those flow patterns are linked to the arrangement and the size of the overlapping scales within the array. Because of the velocity streaks, total drag reduction is observed when the scale height is small relative to the boundary layer thickness, i.e. less than 10%. Flow simulations were compared with surface oil-flow visualisations on the physical model of the biomimetic surface placed in a flow channel. The results show an excellent agreement in the size and arrangement of the streaky structures. The existence of streaks is also shown on sea bass and common carp (*Cyprinus carpio*) by surface flow visualisation. From comparisons with recent literature on micro-roughness effects on laminar boundary layer flows, it is hypothesised that the fish scales could delay transition, which would further reduce the drag.

KEY WORDS: Fish scale, Streaks, Hydrodynamics

INTRODUCTION

All bodies that move through a surrounding fluid will generate a boundary layer over their surface because of the no-slip condition at the boundary of the fluid region (‘the wall’) (Schlichting and Gersten, 2017). This boundary layer is a region of concentrated vorticity, which shears the fluid near the body surface and the work done to shear the fluid is the measure of the energy spent in locomotion (Anderson et al., 2001). The shear stress near the surface depends on the velocity gradient at the wall and the type of boundary layer, both of which exist near the surface (Schlichting and Gersten, 2017). If the boundary layer is laminar, the drag will be low, but it is more prone to separation at adverse pressure gradients, which increases the pressure drag. A turbulent boundary layer produces more skin friction because of the additional turbulent stress near the surface; however, it can sustain a much stronger adverse pressure gradient, which allows operation in off-design conditions (Schlichting and Gersten, 2017). There is always a trade-off in design to maintain the initial boundary layer laminar for the maximum extent so that the skin friction drag is reduced (Selig et al., 1995) and changing quickly to turbulent boundary layers in areas that are prone to separation. For marine vehicles, one may overcome larger friction by modifying the surface with a hydrophobic coating so that the fluid slips along the surface in contrast to the no-slip condition of an uncoated one. As a consequence, the skin friction is reduced, which, in turn, reduces the net drag of the body (Ou et al., 2004; Daniello et al., 2009). This technology was motivated by the lotus effect (reviewed by Bhushan and Jung, 2006) and contributes to self-cleaning of the surface, which could reduce fouling in the marine environment (Bhushan et al., 2009). For large fast swimmers such as sharks, there have been numerous experimental and computational studies on the skin denticles (Wen et al., 2014; Oeffner and Lauder, 2012; Domel et al., 2018). These were found to manipulate the near skin flow to reduce turbulent drag. However, little work has been done on smaller and slower fish with laminar or transitional boundary layers and the role of different arrangements and patterns of fish scales on their swimming behaviour and hydrodynamics. Lauder et al. (2016) have claimed that there is still no detailed proof on the hydrodynamic role of fish scales. Wainwright and Lauder (2016) measured the scale morphology of bluegill sunfish (*Lepomis macrochirus*) with GelSight technology and speculated about the hydrodynamic function of the scales. Later, using the same technology, the surface topography of various fish species was measured with and without the mucus layer (Wainwright et al., 2017). Some physical characteristics of scales from grass carp (*Ctenopharyngodon idellus*) were measured and manufactured as a bionic surface. An indication of drag reduction of about 3% was reported (Wu et al., 2018) and the authors concluded that a water-trapping mechanism was responsible for this reduction, mainly due to flow separation behind the scales. No further details were given on the flow structure. In addition, the scales were not overlapping but treated as individual elements. The present paper aims to reproduce a more realistic fish surface based on the statistics of scale measurements and reproduction of the overlapping scale array along the body. We focus our studies on the European bass (*Dicentrarchus labrax*), which is commonly found in Mediterranean, North African and North Atlantic coastal water regions. The fish scale pattern and array overlap are almost homogeneous over the length of the body.

MATERIALS AND METHODS

Fish samples

European bass [*Dicentrarchus labrax* (Linnaeus 1758)] and common carp (*Cyprinus carpio* Linnaeus 1758) were collected from local fishmongers (Moxon’s Fishmonger, Islington, London, UK and East Ham Fresh Fish Ltd, London, UK). Five individuals of both sexes (total length of ≥33 cm) were used for the experiments. Sampling occurred from the pectoral region to the caudal region at 10 equally spaced intervals between point S and E as shown in Fig. 1A. The skin of the fish was cleaned repeatedly with a 70% ethanol solution to remove the mucus layer. Immediately after cleaning, scale samples were removed from the skin and placed on object slides. Samples were analysed with a digital microscope

[1]Department of Mechanical Engineering, City, University of London, London EC1V 0HB, UK. [2]School of Life Sciences, University of Keele, Keele ST5 5BJ, UK.

*Author for correspondence (muthukumar.muthuramalingam@city.ac.uk)

M.M., 0000-0003-0018-3890

Received 26 April 2019; Accepted 28 July 2019

Journal of Experimental Biology (2019) 222, jeb205963. doi:10.1242/jeb.205963

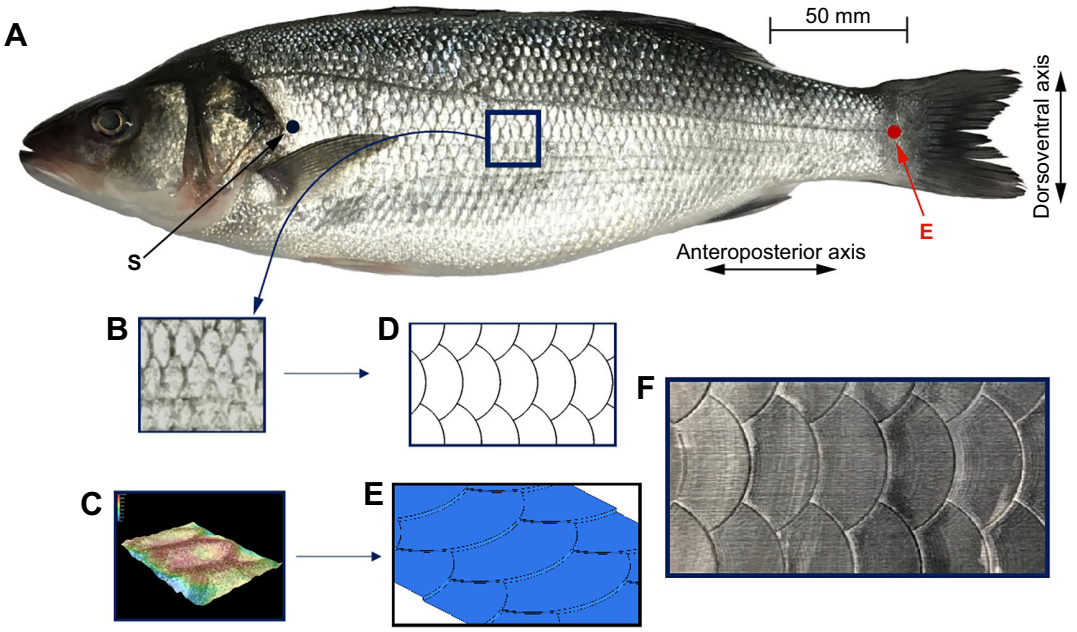

Fig. 1. Microscope images and computer-aided design (CAD) replication of sea bass fish scales. (A) Image of sea bass. Points S and E show the regions where measurements were taken. (B) Top view of the scales. (C) Topographical view obtained by scanning with a digital microscope. (D) Top view of replicated CAD model. (E) Isometric view of CAD model. (F) Top view of 3D printed model of sea bass scales.

(VHX-700FE series, Keyence) using the 3D mapping feature of the built-in software (see Figs S1–S3 for microscopic measurements and detailed CAD model). This allowed us to scan the 3D contour and to store the coordinates for later replication of the scale surface in computer-aided design (CAD) software. The 2D images and the 3D topographical scan from the microscope, the replicated CAD design and the 3D printed surface of fish scale array are shown in Fig. 1B–F. The physical model was scaled 10 times larger than the actual size, which is a practical scale for experimental studies in the flow channel (Panton, 2013). Experiments with up- or down-scaled models are a common strategy in hydrodynamic and aerodynamic research based on the boundary layer scaling laws (Fig. S4).

Computational methodology

The computational domain and the boundary conditions are shown in Fig. 2A. For comparison with the experiments, the length-scale of reference herein is the same as for the 10-times upscaled physical model. The dimensions in x (anteroposterior axis), y (dorsoventral axis) and z (lateral axis) directions were 250 mm, 200 mm and 80 mm. The array of scales was designed with 10 rows along the x-direction and 5 rows in the y-direction. The scale height from the base varies in both the x- and y-direction. Hence, the height of a scale at a given position $P_{x,y}$ is defined as h_P, whereas the maximum height of the scale in the centre line (h_s) is about 1 mm, which corresponds to a 10-times enlarged value compared with the measured value of 100 µm. At the inlet to the domain, a laminar Blasius-type boundary layer velocity profile with a boundary layer thickness (δ) of 10 mm was imposed. This profile can be approximated according to Pohlhausen (Panton, 2013) as a second order polynomial profile given by:

$$\frac{u(y)}{U_\infty} = A\left(\frac{y}{\delta}\right) + B\left(\frac{y}{\delta}\right)^2, \quad (1)$$

$$\delta(x) = \frac{5 \cdot x}{\sqrt{Re_x}}, \quad (2)$$

$$Re_x = \frac{\rho \cdot U_\infty \cdot x}{\mu}, \quad (3)$$

where A and B are the coefficients based on the free stream velocity (U_∞=0.1 ms^{-1}) and the boundary layer thickness (δ=10 mm) at the inlet (A=2, B=−1). The boundary layer thickness given by Eqn 2 corresponds to a flat plate Reynolds number of about Re_{xo}=33,000 with an imaginary inlet length of x_o=333 mm from the leading edge of a flat plate until it reaches the inlet of the domain, where the Reynolds number (Re_x) is defined by Eqn 3. All the other side walls except for the floor and the fish scale array were specified with free slip conditions, i.e. zero wall-shear. The domain was meshed with 18 million tetrahedral elements with 10 prism layers near the wall with a first cell value of 0.06 mm. To study the effect of scale height relative to boundary layer thickness on total drag, different boundary layer thickness at the entrance were simulated. Therefore, the inlet domain was extended for 200 mm upstream as shown in Fig. 2B and different boundary layer thicknesses at the new inlet was specified as 5, 10 and 15 mm. The problem was solved using the steady state pressure based laminar solver in ANSYS Fluent 19.0 with a second-order upwind method for momentum equation. Water was used as the continuum fluid in this computational fluid dynamics (CFD) study with a density (ρ) of 1000 kg m^{-3} and a dynamic viscosity (µ) of 0.001 kg m^{-1} s^{-1}.

Surface flow visualisation on biomimetic fish scale array

The fish scale array with dimensions explained in the previous section was 3D printed with ABS plastic using fused deposition modelling (FDM) (Raise 3D). For manufacturing, the base layer thickness needed to be 4 mm to ensure stable handling. The model was placed on the floor of a wind tunnel (PARK Research Centre, Coimbatore, India) in the test section (cross-section of 450 mm and 600 mm width). To reduce the disturbance of the step at the leading edge, a chamfered flat plate (size 250 mm×200 mm×4 mm) was

Journal of Experimental Biology (2019) 222, jeb205963. doi:10.1242/jeb.205963

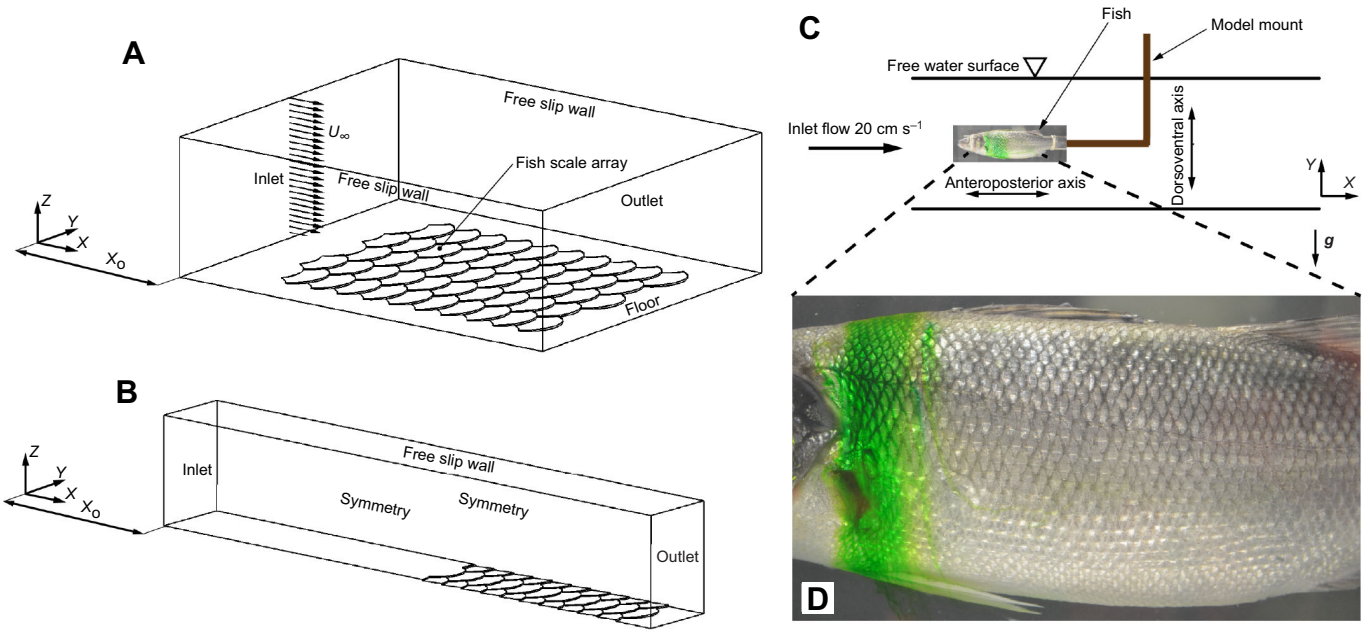

Fig. 2. Computational domain and experimental set-up to assess the flow over model and real fish scales. (A) Configuration of the fish-scale array in computational fluid dynamics (CFD) similar to the condition of the physical model of the scale array at the bottom wall of the wind tunnel. Note that the velocity vector represents the inlet profile with free-stream velocity parallel to the *x*-axis in a positive direction (anteroposterior direction). *y*-axis represents the spanwise (dorsoventral direction) and *z*-axis represents wall normal direction. (B) CFD domain with symmetry conditions to simulate the drag variation with no end effects. In both the figures x_o is the imaginary length from the leading edge of the plate to the inlet of the domain. (C) Schematic diagram of the experimental set-up. (D) Dye coating on the surface of the fish.

placed upstream and downstream such that the region with the scale array was flush with the wall. Surface oil-flow visualisation was performed with a mixture of titanium dioxide and kerosene with a drop of soap oil to avoid clustering of particles. For more details of this visualisation, see Merzkirch (2012). Before starting the wind tunnel, the model was painted with the mixture in the region downstream of the scale array. Thereafter, the tunnel flow was started to a free-stream velocity of 12 m s^{-1}, which gave a boundary layer thickness of about 10 mm at the entrance to the scales. Wind transports the dye according to the local wall shear. A camera mounted on the top of the tunnel captured this process.

Surface flow visualisation on real fish skin

Flow visualisation experiments on real fish (lifeless) were conducted in a return type open surface water tunnel at City, University of London. The test section is 40 cm×50 cm×120 cm (width×depth×length) and transparent in all the sides to provide an optical access for flow studies. Inlet flow velocity was set at 20 cm s^{-1}. Sea bass of length (L≈340 mm) and common carp of length (L≈320 mm) were used in this study. Each fish was mounted on an L-shaped string at the centre of the water tunnel from the base (see Fig. 2C). Synthetic food colour was mixed with few drops of oil and coated on the surface of the body just downstream of the snout of the fish as shown in Fig. 2D. The ratio between the viscosity of the water and the oil lies in the range discussed by Squire (1961); hence, the effect of oil flow on the flow dynamics was very small. The motion of the oil-mixture was captured with a high speed camera which was mounted outside the water tunnel.

RESULTS

Flow data obtained from the CFD results are first presented as velocity fields and profiles. Fig. 3A shows colour-coded contours of constant streamwise velocity (normalised with the free-stream velocity) in a wall-parallel plane at a distance of 0.25δ. At the inlet, the velocity is uniform along the spanwise direction (*y*-direction), whereas along the flow direction over the scales, there is a periodic velocity variation in spanwise direction. Low velocity regions emerged in the direction of the centre lines of the scales (yellow arrows). In comparison, high velocity regions (red arrows) are seen along the regions where the scales overlap. These high velocity and low velocity regions are referred to hereafter as streaks. These structures are linked in number, location and size, with the overlap regions along the dorsoventral axis over the surface.

Further information on the variation of the velocity in the streaks is demonstrated in Fig. 3B. It shows spanwise profiles of the streamwise velocity at the location x=x_o+190 mm (8th scale in the row along streamwise direction from the inlet) for different wall normal locations. At a wall normal location of 0.15δ, the velocity variation is around 10% of U_∞ between the peak (local max) and valley (local min) in the profile. Given this difference, the streak amplitude is calculated from Siconolfi et al. (2015):

$$A_{ST} = \left[\max_y\{U(X,y,z)\} - \min_y\{U(X,y,z)\}/(2U_\infty)\right]. \quad (4)$$

As seen from the different profiles, the location of peaks and valleys do not change with wall normal position, therefore the streaks extend over most of the boundary layer thickness in a coherent way. The streak amplitude A_{ST} is plotted along the wall normal location in Fig. 4 and it can be seen that the streak amplitude is maximum within the first 20% of the boundary layer thickness with a value of 4.5% of U_∞. As the distance from the wall increases, the streak amplitude decreases monotonically until the displacement effect of the scales has died out at the outer edge of the boundary layer (1.05δ from the wall).

Journal of Experimental Biology (2019) 222, jeb205963. doi:10.1242/jeb.205963

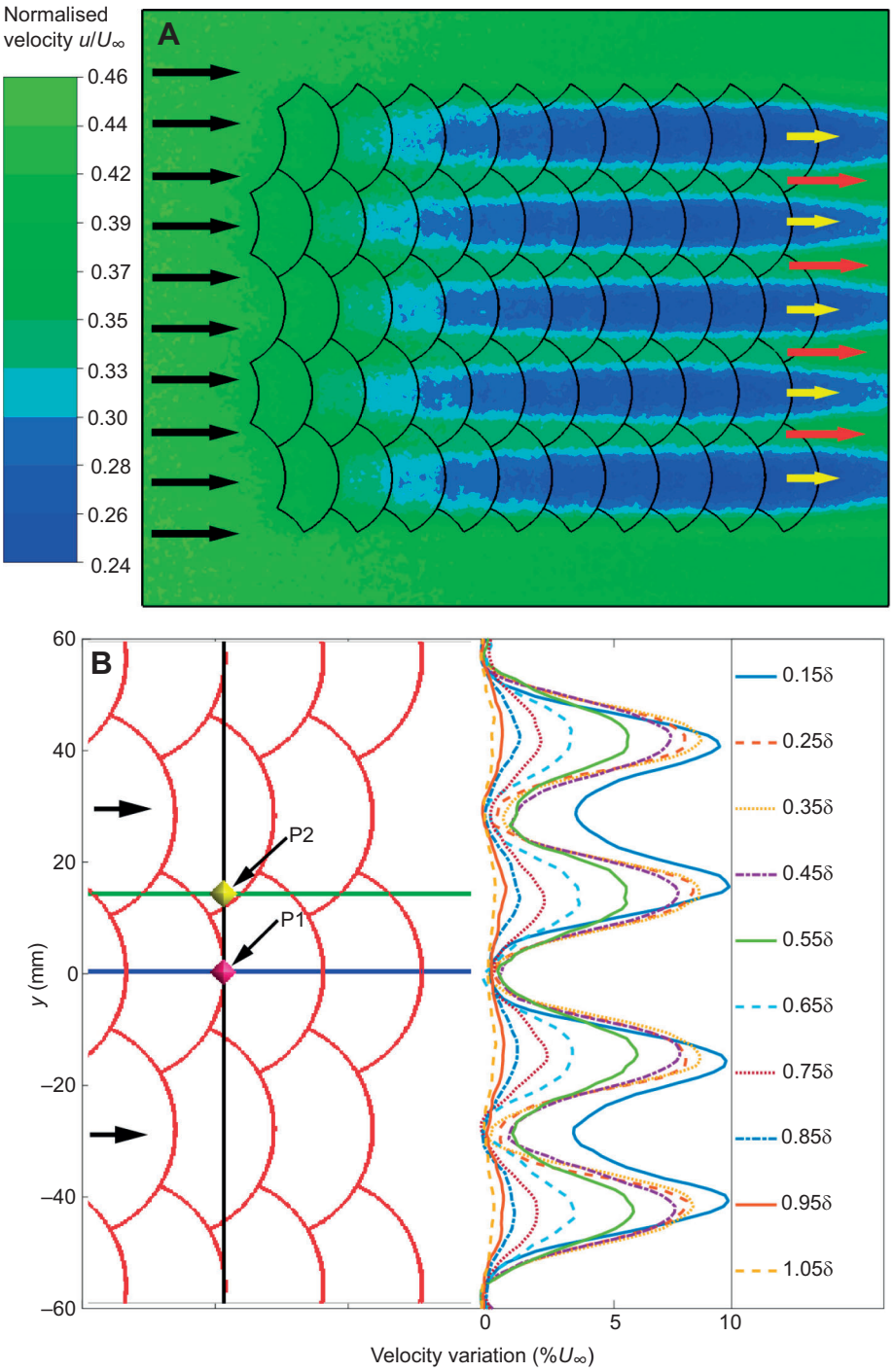

Fig. 3. Velocity contour and velocity profiles over model fish scales. (A) Normalised velocity contour at a wall-parallel plane at a distance of z=0.25δ from the surface. Arrows indicate flow direction. Note that the black arrows at the inlet are uniform in length, while red and yellow arrows at the outlet differ in length. (B) Velocity variation in spanwise direction at various wall-normal distances in the boundary layer. Scale array is shown in red. Blue line represents a centre line of a row of scales. Green line represents the overlap region between the scales. Black line represents a location in the x-direction at 190 mm from inlet. P1 and P2 are probe points at 190 mm from inlet on centre line region and overlap region. Black arrows indicate mean flow direction.

Experimental flow visualisation images of the streaks behind the fish scale array are shown in Fig. 5A. As the particle mixture coated on the surface moves according to the direction and the magnitude of wall-shear, the mixture moves farther in the regions of high shear than in regions of low shear. Therefore, the flow produces streaky patterns on the surface with different lengths downstream of the scale array (Fig. 5A); the red dashed lines depict the orientation of the streaks relative to the pattern of the scale array. It is clearly seen that the high-speed streaks are formed in the overlap regions as claimed from the CFD results. For better comparison with the CFD results, the surface flow visualisation over the scale array is overlaid with surface streamlines from CFD (see Fig. 5B), which is discussed later. Fig. 5C shows the result from the surface flow visualisation experiment on sea bass where two clear streaks are visible on the surface where the scales overlap. The same experiment was repeated with the common carp, which has a larger scale size but with a similar overlap pattern when compared with sea bass. In this case, four streaks were clearly visible along the overlap region of the scales (Fig. 5D). Hence the number of overlap regions defines the number of streaks produced on the surface of the fish. The results from the biomimetic scale array is in excellent agreement with the flow over the real fish surface.

Fig. 6 shows the variation of the normalised velocity profile at two locations along the span at the 8th scale row (probe point

Journal of Experimental Biology (2019) 222, jeb205963. doi:10.1242/jeb.205963

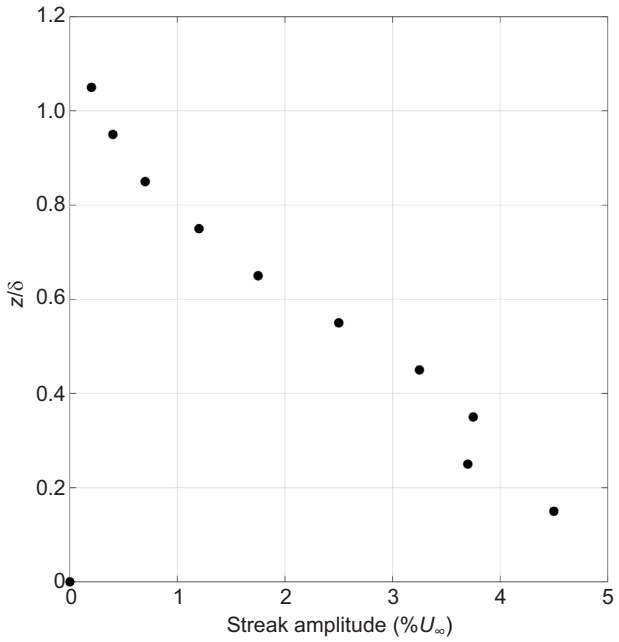

Fig. 4. Variation of streak amplitude along wall-normal direction for model fish scales. Measurements were made 190 mm from water inlet (along black line shown in Fig. 3B).

locations P1 and P2, compare Fig. 3B). In the absolute coordinate system (Fig. 6A) there is a shift in z-direction because of the variation in the scale height h_P along the span of the surface. When the profiles are plotted in the body relative system ($z=z-h_P$), the difference along the wall normal direction (Fig. 6B) becomes more obvious. With the scales on the surface, the gradient of the velocity near the wall gets steeper in the location discussed here (at the probe points P1 and P2). This is concluded from the comparison to the Blasius velocity profile for a smooth flat plate (dashed black line). However, the boundary layer thickness is approximately the same. Fig. 6C shows the variation of the dimensionless velocity profile at three locations: at P2, four scales upstream from P2 (P2-4S) and at the outlet of the computational domain. Dimensionless velocity u^+ is defined by $u^+=u/u_\tau$ where, frictional velocity at the wall $u_\tau=\sqrt{(\tau_w/\rho)}$ and wall coordinate y^+ is defined by $\rho u_\tau y/u_\tau$. It is evident that at all three locations the profile is similar to the reference Blasius profile (dotted red line) suggesting that the velocity variation is laminar at all locations. This suggests that scales change the profile shape inside the boundary layer region but do not change the boundary layer thickness (nevertheless affecting the displacement and momentum thickness). Turbulent boundary layer velocity profile (log law profile) for flow over a flat plate is shown for comparison.

The surface streamline picture generated from the CFD results is shown in Fig. 7A. In the centre line of the scales, the flow mostly follows the direction of the main flow. Section X–X is enlarged and the cross-sectional flow in the centre of the scales is shown in Fig. 7B. The flow follows the small slope caused by the tilt angle of the scale until it separates from the sharp edge on the scales and reattaches further downstream at approximately 2.5 times the scale height (h_s) on the surface as a laminar boundary layer. This non-dimensional reattachment length is very similar to the value reported in horizontal backward facing step flows if the Reynolds number defined with the step height and free stream velocity is around 100 for the given flow situation (Goldstein et al., 1970). This separated flow region behind the step is visible from the dividing streamline (shown as thick dashed line in Fig. 7B). Also, from the surface flow visualisation, the separated flow region behind the edge of the scales can be observed by the white patches due to the accumulation of the particles (see Fig. 5B). These white patched regions match in size and location with the flow reversal zones in the CFD. When the fluid moves along the scales, the streamwise component of velocity is reduced in the central region of the scale by the large separated zone, as explained above. This causes a spanwise pressure gradient and forces the fluid to move from the central region of the scales to the overlapping region. This movement is seen in the zig-zag pattern (shown by blue arrows in Fig. 7A) with larger spanwise components of fluid motion. The spanwise flow towards the overlapping region produces a higher streamwise velocity because of mass conservation. This causes high-speed streaks in these regions. In addition, it is evident that the flow reversal is reduced compared with the cross-section at the central region of the scales. This is the root cause of producing low speed and high-speed streaks.

Fig. 8 shows the surface streamlines on the scale array along with cores of intense vortices visualised by isosurfaces of the Q value (Jeong and Hussain, 1995). The colours of the isosurfaces indicate the streamwise helicity which is defined as $(U_x \cdot \omega_x)$, where ω_x is the vorticity component along the x-direction. The yellow colour defines the region in which the vortex direction is counter clockwise (CCW) with respect to the x-axis direction (i.e. mean flow direction represented by a white straight arrow in Fig. 8.), similarly, the blue colour defines the clockwise (CW) vortex direction. It also displays the cross-flow velocity fields on planes parallel to the Y–Z plane near the scale overlap region for two consecutive scales. The vortex in the central region of the scales (i.e. white colour vortex core) reflects the reversed flow region behind the step. There, the flow direction remains nearly aligned with the mean flow. In comparison, when the flow moves downstream in the overlap region it is affected by successive vortices with alternating direction switching from CCW to CW and vice versa. This causes the streamlines in the overlap region to generate a zig-zag pattern, as illustrated in Fig. 7A.

Skin friction and total drag

As previously mentioned, the scales modulate the near wall flow with streaks that will change the wall shear stress (τ_w) distribution on the surface when compared with flow over smooth flat plate. To analyse this effect, the skin friction coefficient C_{fx} defined by Eqn 5 is plotted along the centre line (see blue horizontal line in Fig. 3B) together with the surface profile variation in Fig. 9A. In addition, the figure shows the profile of the theoretical skin friction coefficient ($C_{fx,theory}$) for a smooth flat plate case, given in Eqn 6. Along the initial smooth part of the surface until 25 mm the skin friction coefficient follows the theoretical skin friction coefficient. As it enters the scale region, initially the skin friction drops because of the adverse pressure gradient caused by the first wedge. Over the scale, it increases again because of the local acceleration until it reaches the maximum at the edge of the scale. Then, C_{fx} drops to a negative value because of the recirculation region explained in Fig. 7B. Once the flow reattaches, the skin friction becomes positive again and increases until it reaches the peak as it approaches the edge of the next scale. This process repeats itself in flow direction with the succession of scales. The same process happens in the overlap region, but here, for a single scale length, the process happens twice because of two small steps formed by the adjacent scales in the lateral overlap region (note the difference in the scale profile in the central region in Fig. 9A and the scale profile in the overlap region in Fig. 9B). Additionally, the streamwise wall shear does not reach

Journal of Experimental Biology (2019) 222, jeb205963. doi:10.1242/jeb.205963

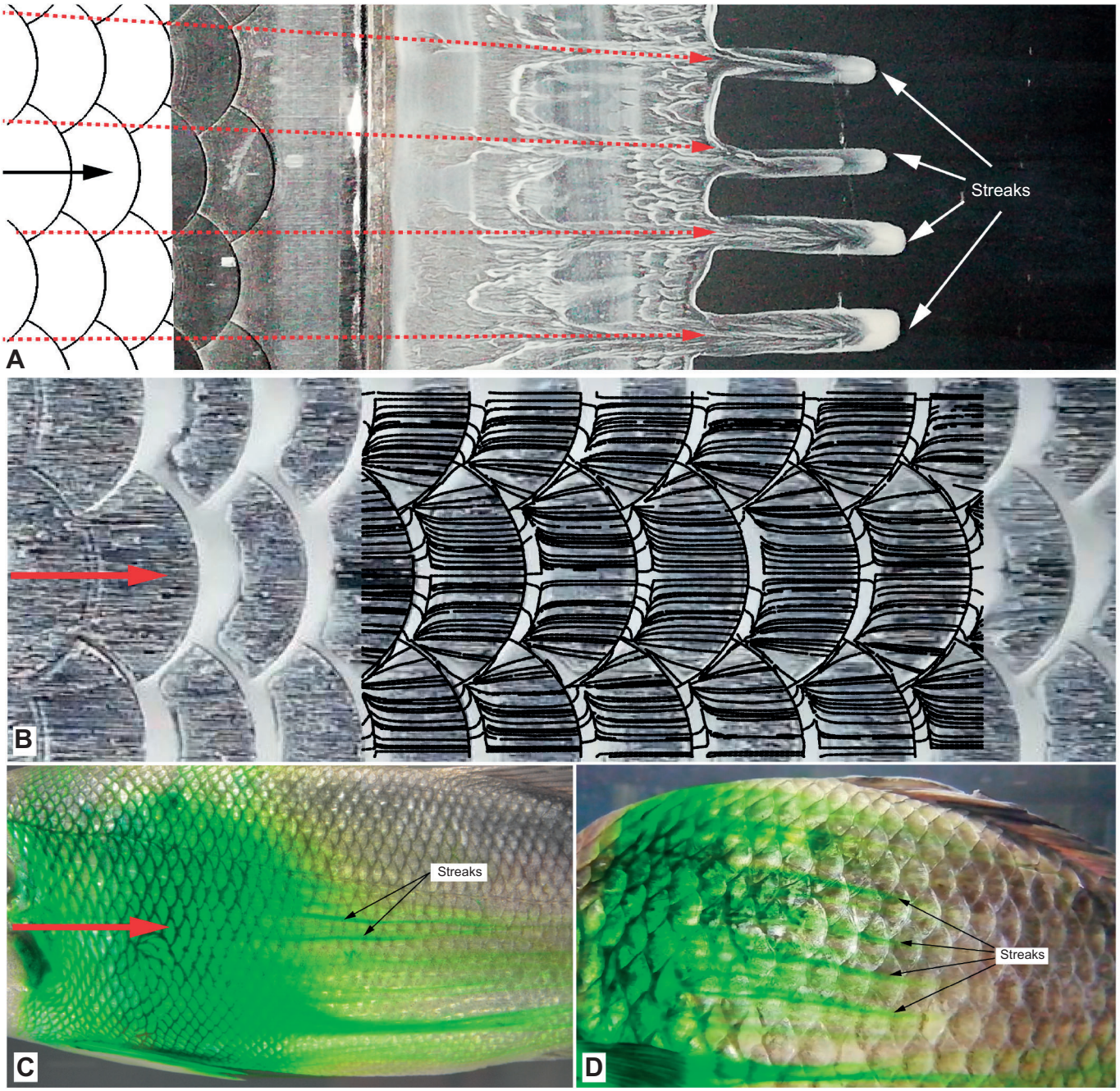

Fig. 5. Surface flow visualisation on model fish scales and on real fish scales. (A) Black arrow represents mean flow direction. An oil mixture was painted in the region downstream of the scales to highlight the generation of the streaks. 2D top view of the CAD model is merged to get the impression of the arrangement of the scales. The red dashed arrows illustrate the trace of the streaks relative to the arrangement of the scales. (B) Red arrow represents the mean flow direction. Here, the oil mixture was painted directly onto the scales. Surface streamlines from CFD simulation are overlaid to compare the results. Note that the regions of accumulated oil patches match with the regions of flow reversals from computational fluid dynamics (CFD) simulation. (C,D) Oil-flow visualisation on (C) sea bass and (D) common carp. Red arrow in C represents the mean flow direction.

negative values in the valleys as there is no flow reversal in these zones. The shear drag along the central region (determined by the integration of wall shear in the streamwise direction along blue horizontal line in Fig. 3B) gives a 12% reduced value compared with the theoretical drag for a smooth flat plate. In contrast, the overlap region (determined by the integration of wall shear in the streamwise direction along the green horizontal line in Fig. 3B) gives a 5% increase in shear drag. This tendency along the span correlates with the low and high velocity regions, as wall shear stress is directly

Table 1. Dependence of drag force on boundary layer thickness to fish scale height ratio

δ/h_s	C_{dp}	C_{df}	$C_{d,total}$	$C_{d,theory}$	ΔC_{df}%	$\Delta C_{d,total}$%
5	0.000277	0.00448	0.00476	0.00453	−1.03	5.08
10	0.000193	0.00301	0.00320	0.00316	−4.68	1.43
15	0.000129	0.00214	0.00226	0.00236	−9.31	−3.84

Journal of Experimental Biology (2019) 222, jeb205963. doi:10.1242/jeb.205963

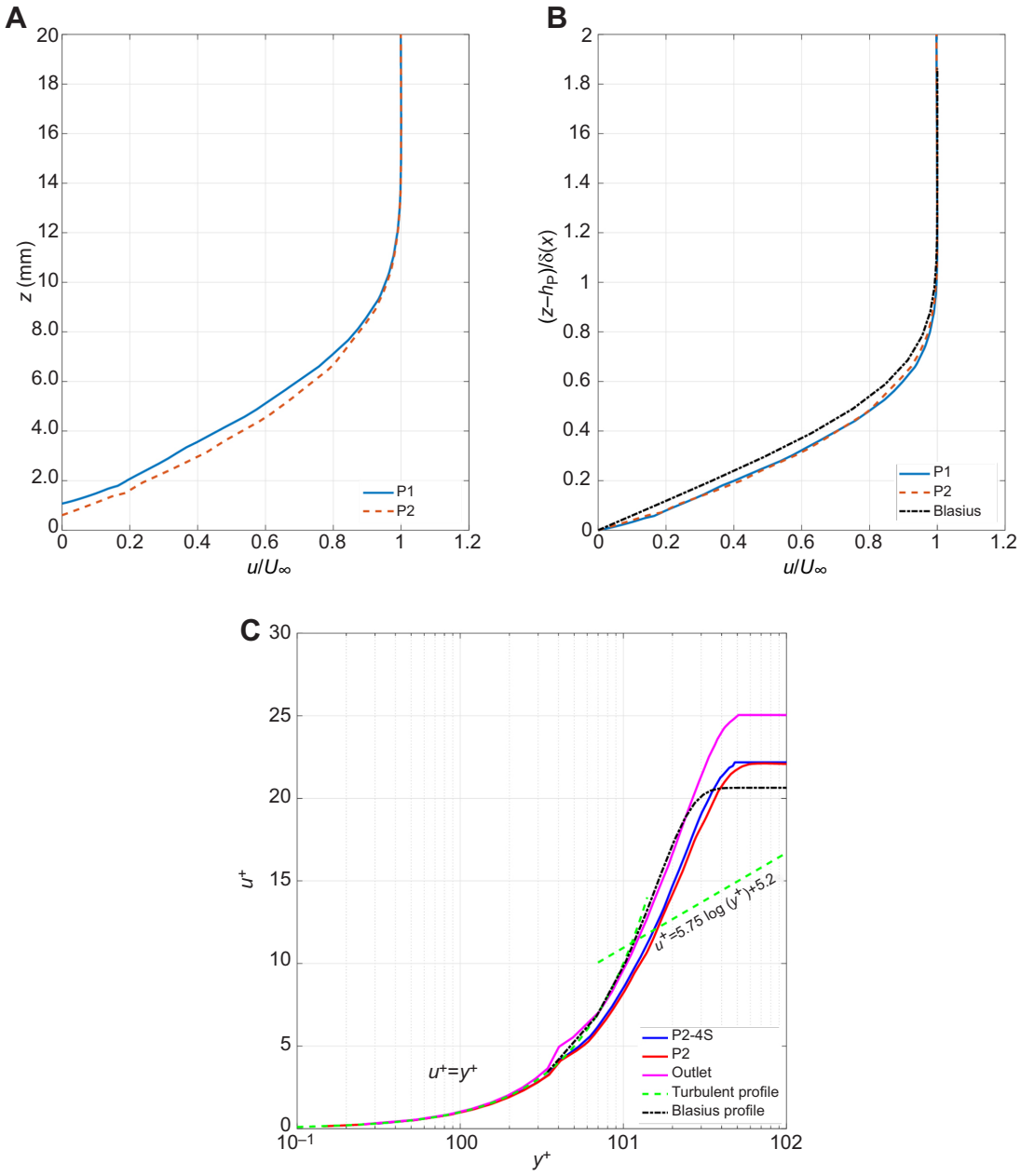

Fig. 6. Boundary layer profiles of model fish scales. (A) Normalised velocity profiles in the absolute coordinate system. Measurements were made at two locations (P1 and P2 in Fig. 3B). Note that the shift in velocity profiles along the *z*-direction is due to the change in scale height h_P for the different probe points P. (B) Normalised velocity in the body coordinate system with Blasius laminar boundary layer profile along a smooth flat plate. (C) Dimensionless velocity profile at three locations: P2, four scales upstream of P2 (P2-4S) and at outlet. Green dashed lines show turbulent velocity profile for flow over a flat plate $u^+=y^+$ and $u^+=5.75\log(y^+)+5.2$.

proportional to the velocity gradient. The integral over the total surface leads to the total friction drag, which is a net effect of the streaks. As we introduce a surface which is not smooth, the total drag is the sum of the friction and the pressure drag. The latter depends on the wake deficit behind the step of the scale because of the separated flow regions. Both need to be taken into account from the CFD results to investigate the net effect on possible total drag reduction.

In order to investigate the relative contributions of friction and pressure drag over the skin, we varied the boundary layer thickness (δ) relative to fish scale height (h_s) as reported in Table 1. The inlet boundary layer thickness in the CFD domain was increased in steps from δ=5, 10 and 15 mm, respectively, with a free stream velocity (U_∞) value of 0.1 m s^{-1}. Drag coefficients were calculated using the drag force values obtained from CFD. The change in friction drag and total drag coefficients is given in Eqn 7. The theoretical drag coefficient ($C_{d,theory}$) is calculated by integrating the skin friction coefficient ($C_{fx,theory}$) along the *x*-direction:

$$C_{fx} = \frac{\tau_w}{0.5 \cdot \rho \cdot U_\infty^2}, \tag{5}$$

$$C_{fx,theory} = \frac{0.73}{\sqrt{Re_x}}, \tag{6}$$

$$\Delta C_{df}\% = \frac{(C_{df} - C_{d,theory})}{C_{d,theory}} \times 100$$

$$\Delta C_{d,tot}(\%) = \frac{(C_{d,tot} - C_{d,theory})}{C_{d,theory}} \times 100. \tag{7}$$

Journal of Experimental Biology (2019) 222, jeb205963. doi:10.1242/jeb.205963

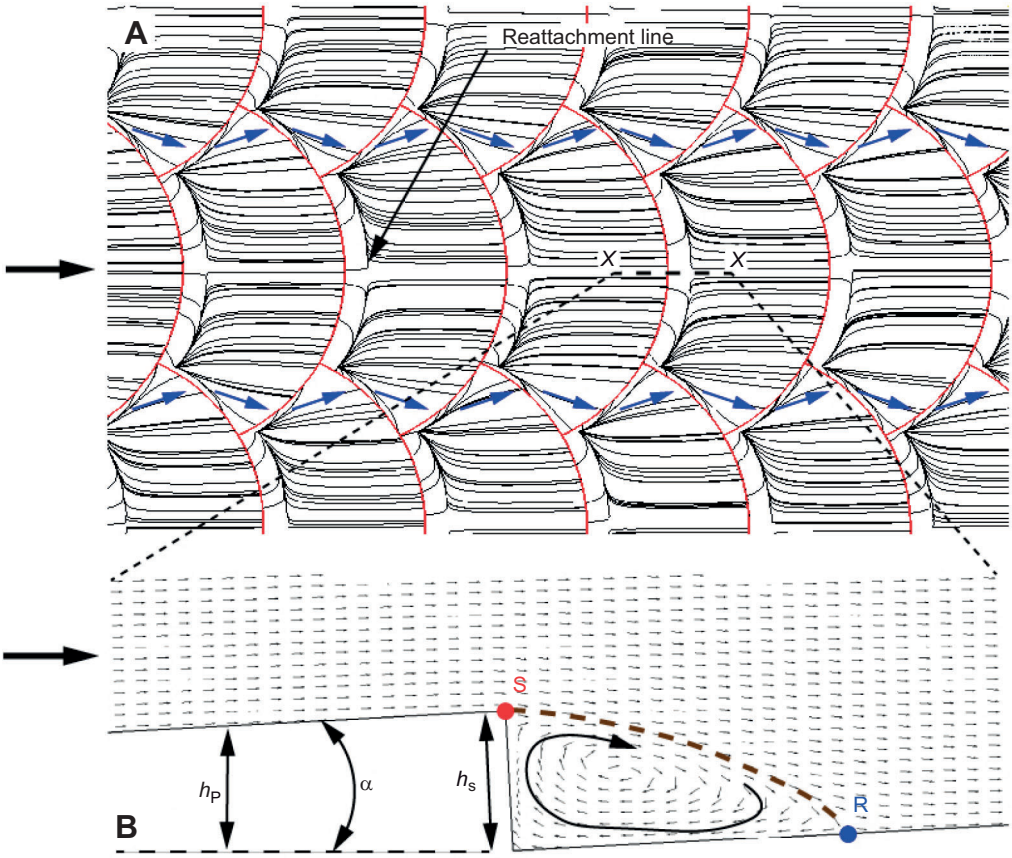

Fig. 7. Surface streamline and vector plots on model fish scales from computational fluid dynamics (CFD) simulation. (A) Top view of surface streamline over the scales. Note the zig-zag motion along the overlap region compared with the parallel flow at the central regions of the scales. (B) Vector field in the *x*–*z* cross sectional plane along the central region of the scale at line *X*–*X* (vectors indicate only direction and not magnitude). h_s=1 mm and α=3 deg. S and R represents the separation and reattachment of the flow streamlines, respectively. Thick dashed line between S and R indicates the region of recirculating flow with an arrow indicating the direction of rotation. In both drawings the black arrow on the left indicates the mean flow direction.

For all the three cases, the change in friction drag (ΔC_{df}%) relative to the smooth flat plate is negative, indicating that the scales are efficient in reducing skin friction. This effect increases with increasing boundary layer thickness to scale height ratio. However, the total drag is only reduced for the third case ($\Delta C_{d,total}$=−3.84%) when δ/h_s ratio is 15. This is the typical ratio between the boundary layer thickness and the scale height in cruising conditions of the flow around the fish and will be explained in the Discussion.

DISCUSSION

In this paper, 3D microscopic measurements of the scales on the European bass fish are presented. Based on the data statistics, a biomimetic scale array was replicated with the use of Computer Aided Design and 3D printing. The study differs from previous ones on biomimetic scales (Dou et al., 2012; Wainwright et al., 2017; Wainwright and Lauder, 2017) in that it is the first for European bass and the first using a typical 3D curvature of the scales with an additional overlap pattern. Flow over the scale array was analysed using computational fluid dynamics and experimental results were obtained from the surface flow visualisation. Excellent qualitative agreement was found, showing the formation of alternating high-speed and low-speed streaks along the span, which suggests that the location, size and arrangement of the streaks are linked with the overlap pattern of the scales. The experimentally validated CFD data

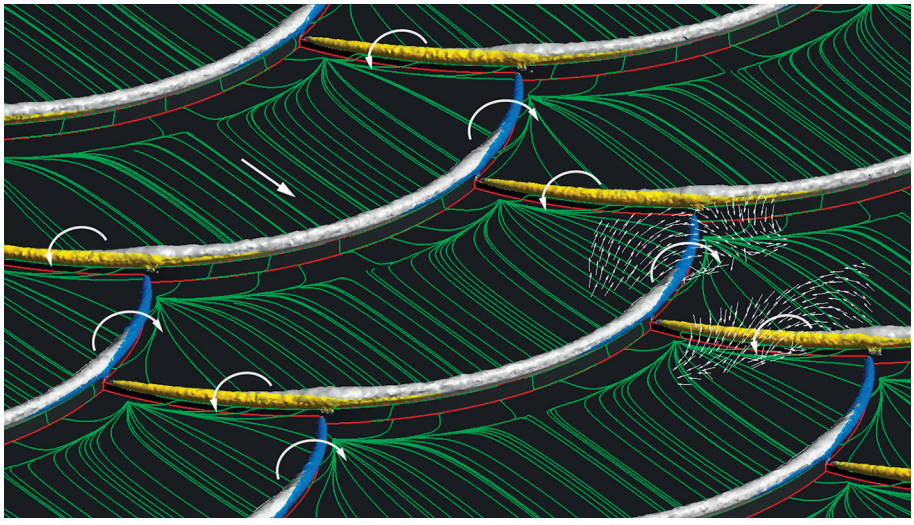

Fig. 8. Surface streamline plot with direction of vortices on model fish scales. Vector plots at the overlap region for two consecutive scale rows. Helicity coloured in yellow for positive (vortex direction counter clockwise) and blue for negative (vortex direction clockwise). Other rotational vectors are based on the colouring of vortices. Vortices are identified with *Q* criterion. White straight arrow represents the mean flow direction.

Journal of Experimental Biology (2019) 222, jeb205963. doi:10.1242/jeb.205963

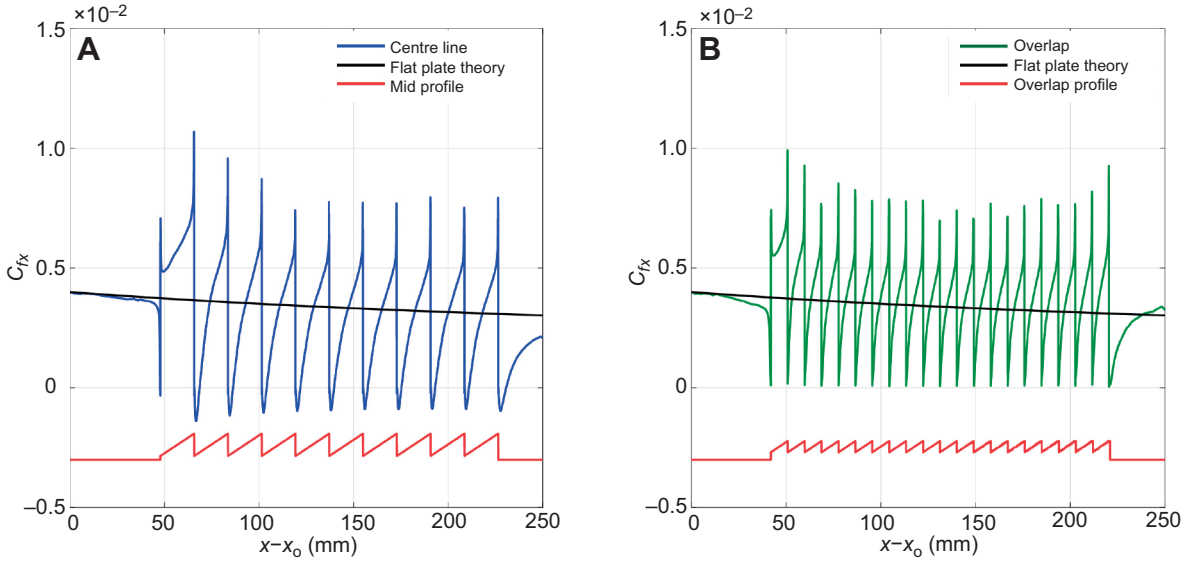

Fig. 9. Variation of the skin friction coefficient along the *x*-direction at two locations on model fish scales. (A) Variation in C_{fx} along the scale centre line (see blue line in Fig. 3B). (B) Variation in C_{fx} along the scale overlap region (see green line in Fig. 3B). Red lines represent variation of the *z* coordinate in the *x*-direction along corresponding locations (not to scale). Black lines represent the variation of $C_{fx,theory}$ for flat plate boundary layer by Eqn 5. x_o (333 mm) is the imaginary length before the inlet of the domain.

further allows us to draw conclusions about the total drag of the surface, which is relatively difficult to obtain experimentally. The derived drag values show that the overlapping scale arrays are able to reduce the body drag if their characteristic step height is sufficiently small (at least one order of magnitude) compared with the local boundary layer thickness. If this conclusion holds for typical flow conditions and size of the scales for European bass, the consequence would be a reduction of total drag, hence costing less energy to the fish whilst cruising. Below, we discuss the possible relevance of this finding to the situation of sea bass in steady swimming conditions, including a critical review of the limitations of the study.

Mucus layer and transport

Any mucus on the scales needs to be washed away for optical reasons before scales can be assessed using microscopy. It is known for similar fish species that the mucus only covers the microstructures of the scales such as circulae and the ridges that connect the ctenii; therefore, the overall shape of the scales is not affected by the wash-out procedure (see also the conclusion by Wainwright et al., 2017). Additionally, from the Rosen–Cornford hypothesis, the mucus layer is reluctant to lower friction (laminar boundary layer) and could be broken and mixed at the aft portion of the fish where turbulence could set in (Rosen and Cornford, 1971). Thus, the flow dynamics is representative for the natural situation of the scales in the flow and our assumption holds in the areas where laminar boundary layers prevail during swimming.

The observed recirculating flow near the central region of the scales might be helpful in retaining the mucus and reducing the mucus secretion rate if the mucus layer breaks from the surface. This inference is supported from the fact that in the surface flow visualisation experiments the mixture was largely trapped in these regions. This is comparable with the results on flow over grass carp fish scales (Wu et al., 2018).

Swimming speed and Reynolds number

The swimming speed of European bass is proportional to its body length (Carbonara et al., 2006). For the fishes considered in this study, the swimming speed lies in the range of 1.2–1.4 m s^{-1} corresponding to a Reynolds number (calculated with the full body length *L*) in the range of 4×10^5–6×10^5. This is when transition from laminar to turbulent boundary layer flow sets in according to classical fluid dynamics. As the reference length is the tail end, we can conclude that the boundary layer over the sea bass for most of the body length remains laminar. Direct measurements of the boundary layer on sea bass are not known so far; however, such data exist for comparable fish such as the scup (*Stenotomus chrysops*), a carangiform swimmer, and rainbow trout (*Oncorhynchus mykiss*). Scup have mostly an attached laminar boundary layer over their body for most of the time and incipient separation appears only for short time intervals in the swimming cycle (Anderson et al., 2001). PIV analysis on swimming rainbow trout at a Reynolds number of 4×10^5 revealed a laminar boundary layer with transition to turbulence in the caudal region (Yanase and Saarenrinne, 2015). Hence, the laminar CFD analysis performed in this study is representative for the effect of fish scales on typical European bass.

For the total drag of the biomimetic surface, a drag reduction was only observed when the scale step height was sufficiently small relative to the local boundary layer thickness (one order of magnitude). At a swimming speed of 1.2 m s^{-1} and for a fish length of 300 mm, the boundary layer thickness will be about 1.5 mm at the middle of the fish body (from Eqn 2) measured from the snout of the fish to the begin of the caudal fin (see Figs S5 and S6 for the boundary layer thickness on approximated fish body). In this region, the scale height measured from the microscope was about 0.1 mm which gives a boundary layer thickness to scale height ratio (δ/h_s) of 15 and has proven reduction in drag. Interestingly, the boundary layer thickness of scup is also in the same range discussed here. Hence, the study shows, at least for steady swimming conditions, valid implications on total drag reduction due to the presence of overlapping scale arrays. The present work is focused only on the fishes with teleost integument as mentioned in the Introduction and the drag reduction discussed relates to laminar boundary layers. For turbulent boundary layers, the scales from the cartilaginous fishes are known to reduce turbulent drag (Dean and

Bhushan, 2010), which is based on another physcial mechanism. Although those swimmers are typically larger and performing at much higher Reynolds number, the scale thickness is still within 1–5% of the turbulent boundary layer thickness (Afroz et al., 2016). Therefore, the optimum scale thickness (relative to the boundary layer thickness) is not different from our findings.

The size of the fish scale changes linearly with the body length from Lee's equation (El-Nasr, 2017); similarly, the critical swimming speed also increases with length (Carbonara et al., 2006). Hence, the boundary layer thickness to scale height ratio (δ/h_s) remains approximately constant throughout the growing phase. For a constant body length of two species such as tuna and common carp, the swimming speed is higher for tuna and lower for common carp. Correspondingly, the boundary layer thickness will be thinner for tuna and thicker for common carp. This could be the reason for tiny scales on tuna when compared with the bigger scales on common carp. However, a definitive conclusion is only possible with more detailed study of several species.

Relevance of streaks in boundary layer transition

The fish scale pattern can be considered to be distributed roughness placed on a smooth surface. Hence, for these types of roughness elements, the roughness Reynolds number calculated from $Re_k=\rho\cdot u_k\cdot h_s/\mu$ is 20, where u_k is the undisturbed velocity at the maximum roughness height (i.e. scale height h_s). The critical roughness Reynolds number to induce bypass transition is around 250 (Doenhoff and Braslow, 1961; Rizzetta and Visbal, 2007). Therefore, the roughness Reynolds number is more than one order below the critical value. Furthermore, the slope of the scale (α) is 3 deg or 0.052 radians. From Singh and Lumley (1971), if the slope of the roughness element is far less than unity (i.e.$\alpha\ll1$) then the stability of the velocity profiles is increased because of the roughness. This suggests that the fish scales act like micro roughness elements which are placed well inside the boundary layer to produce steady low and high-speed streaks without inducing bypass transition.

Studies of the boundary layer flow over a flat plate have shown that placing arrays of micro-roughness elements on the plate can delay transition (Fransson and Talamelli, 2012; Siconolfi et al., 2015). The effect of those elements is that they produce low-speed and high-speed streaks inside the laminar boundary layer, which delay the non-linear growth of the Tollmien–Schlichting waves (Fransson et al., 2004). Although the mechanisms to generate the streaky pattern might be different (lift-up mechanism of streamwise vortices versus alternating vortices in the overlap regions), the fish-scale array-producing streaks could also lead to a delay in transition.

To summarise, the biomimetic fish scale array produces steady low- and high-speed streaks, which are arranged in spanwise direction in the same pattern as the rows of the overlapping scales. This regular arrangement of streaky structures is known from flow studies on generic boundary layer flows to stabilise the laminar steady state and delay transition to turbulence. As already mentioned, the Reynolds number of the fish considered here lies in the transitional range. Thus, we conclude that steady streaks similar to those observed for the biomimetic scale array are indeed produced by the scales of fish, and help to maintain laminar flow over the fish body. The presented biomimetic surfaces can be engineered to reduce skin friction and delay transition in engineering application. However, this only refers to steady swimming conditions. Undulatory motion of the body during active propulsion plays an additional role in the boundary layer transition. Experiments with an undulatory moving silicone wall in flow show an alternating cycle between re-laminarisation and transition in the trough and at the crest of the body wave (Kunze and Brücker, 2011). As the fish surface can also undergo a bending motion, the overlapping scales can move relative to each other and deploy in regions of strong curvature. From previous measurements of the boundary layer over swimming scup, it is known that the boundary layer remains laminar for most of the body without flow separation even in the adverse pressure gradient region (i.e. aft part of the fish) (Anderson et al., 2001). Therefore, whether the scales also take part in any manipulation of flow separation is still an open question (Duriez et al., 2006). From a technological perspective, artificial surfaces with scales can even be built from flexible material, also addressing the issue of local flow separation.

Acknowledgements

We thank Edward Talboys from City, University of London for help with surface flow visualisation on the real fish (lifeless) and Avin Alexander Jesudoss for help with surface flow visualisation on the fish scale model.

Competing interests

The authors declare no competing or financial interests.

Author contributions

Conceptualization: M.M., L.S.V., C.B.; Methodology: M.M., L.S.V., C.B.; Software: M.M., L.S.V.; Formal analysis: M.M.; Investigation: M.M., C.B.; Data curation: M.M., L.S.V.; Writing - original draft: M.M.; Writing - review & editing: M.M., L.S.V., C.B.; Visualization: M.M.; Supervision: C.B.; Project administration: C.B.; Funding acquisition: C.B.

Funding

This work was funded by BAE Systems and the Royal Academy of Engineering (RCSRF1617\4\11 to C.B.) and Deutsche Forschungsgemeinschaft (BR 1494/32-1 to M.M.).

Supplementary information

Supplementary information available online at
http://jeb.biologists.org/lookup/doi/10.1242/jeb.205963.supplemental

References

Afroz, F., Lang, A., Habegger, M. L., Motta, P. and Hueter, R. (2016). Experimental study of laminar and turbulent boundary layer separation control of shark skin. *Bioinspir. Biomim.* **12**, 016009. doi:10.1088/1748-3190/12/1/016009

Anderson, E., McGillis, W. and Grosenbaugh, M. (2001). The boundary layer of swimming fish. *J. Exp. Biol.* **204**, 81-102.

Bhushan, B. and Jung, Y. C. (2006). Micro- and nanoscale characterization of hydrophobic and hydrophilic leaf surfaces. *Nanotechnology* **17**, 2758-2772. doi:10.1088/0957-4484/17/11/008

Bhushan, B., Jung, Y. C. and Koch, K. (2009). Self-cleaning efficiency of artificial superhydrophobic surfaces. *Langmuir* **25**, 3240-3248. doi:10.1021/la803860d

Carbonara, P., Scolamacchia, M., Spedicato, M., Lembo, G., Zupa, W. and McKinley, R. (2006). Swimming performances as a well being indicator of reared sea-bass dicentrarchus labrax (linnaeus, 1758). preliminary results. *Biol. Mar. Mediterr.* **13**, 488-491. doi:10.1007/978-1-4020-6237-7_25

Daniello, R. J., Waterhouse, N. E. and Rothstein, J. P. (2009). Drag reduction in turbulent flows over superhydrophobic surfaces. *Phys. Fluids* **21**, 085103. doi:10.1063/1.3207885

Dean, B. and Bhushan, B. (2010). Shark-skin surfaces for fluid-drag reduction in turbulent flow: a review. *Philos. Trans. R. Soc. A Math. Phys. Eng. Sci.* **368**, 4775-4806. doi:10.1098/rsta.2010.0201

Doenhoff, A. E. V. and Braslow, A. L. (1961). The effect of distributed surface roughness on laminar flow. In *Boundary Layer and Flow Control* (ed. G. Lachmann), pp. 657-681. Pergamon.

Domel, A. G., Saadat, M., Weaver, J. C., Haj-Hariri, H., Bertoldi, K. and Lauder, G. V. (2018). Shark skin-inspired designs that improve aerodynamic performance. *J. R. Soc. Interface* **15**, 20170828. doi:10.1098/rsif.2017.0828

Dou, Z., Wang, J. and Chen, D. (2012). Bionic research on fish scales for drag reduction. *J. Bionic Eng.* **9**, 457-464. doi:10.1016/S1672-6529(11)60140-6

Duriez, T., Aider, J.-L. and Wesfreid, J. E. (2006). Base flow modification by streamwise vortices: application to the control of separated flows. ASME Conference Proceedings (47519), 791-796.

El-Nasr, T. M. A. (2017). Age and growth of the fish, gerres filamentosus (cuvier, 1829) from hurghada red sea, egypt. *Egypt. J. Aquat. Res.* **43**, 219-227. doi:10.1016/j.ejar.2017.07.003

Fransson, J. H. M. and Talamelli, A. (2012). On the generation of steady streamwise streaks in flat-plate boundary layers. *J. Fluid Mech.* **698**, 211-234. doi:10.1017/jfm.2012.80
Fransson, J. H. M., Brandt, L., Talamelli, A. and Cossu, C. (2004). Experimental and theoretical investigation of the nonmodal growth of steady streaks in a flat plate boundary layer. *Phys. Fluids* **16**, 3627-3638. doi:10.1063/1.1773493
Goldstein, R. J., Eriksen, V. L., Olson, R. M. and Eckert, E. R. G. (1970). Laminar separation, reattachment, and transition of the flow over a downstream-facing step. *J. Basic Eng.* **92**, 732-739. doi:10.1115/1.3425124
Jeong, J. and Hussain, F. (1995). On the identification of a vortex. *J. Fluid Mech.* **285**, 69-94. doi:10.1017/S0022112095000462
Kunze, S. and Brücker, C. (2011). Flow control over an undulating membrane. *Exp. Fluids* **50**, 747-759. doi:10.1007/s00348-010-0981-2
Lauder, G. V., Wainwright, D. K., Domel, A. G., Weaver, J. C., Wen, L. and Bertoldi, K. (2016). Structure, biomimetics, and fluid dynamics of fish skin surfaces. *Phys. Rev. Fluids* **1**, 060502. doi:10.1103/PhysRevFluids.1.060502
Merzkirch, W. (2012). *Flow Visualization, chapter Addition of Foreign materials into Gaseous and Liquid Flows*, pp. 82-88. London: Academic Press.
Oeffner, J. and Lauder, G. V. (2012). The hydrodynamic function of shark skin and two biomimetic applications. *J. Exp. Biol.* **215**, 785-795. doi:10.1242/jeb.063040
Ou, J., Perot, B. and Rothstein, J. P. (2004). Laminar drag reduction in microchannels using ultrahydrophobic surfaces. *Phys. Fluids* **16**, 4635-4643. doi:10.1063/1.1812011
Panton, R. (2013). *Incompressible Flow*. John Wiley and Sons, Ltd.
Rizzetta, D. P. and Visbal, M. R. (2007). Direct numerical simulations of flow past an array of distributed roughness elements. *AIAA J.* **45**, 1967-1976. doi:10.2514/1.25916
Rosen, M. W. and Cornford, N. E. (1971). Fluid friction of fish slimes. *Nature* **234**, 49-51. doi:10.1038/234049a0
Schlichting, H. and Gersten, K. (2017). Fundamentals of boundary layer theory. In *Boundary-Layer Theory* (ed. K. Gersten), pp. 29–50. Springer.
Selig, M. S., Maughmer, M. D. and Somers, D. M. (1995). Natural-laminar-flow airfoil for general-aviation applications. *J. Aircr.* **32**, 710-715. doi:10.2514/3.46781
Siconolfi, L., Camarri, S. and Fransson, J. H. M. (2015). Boundary layer stabilization using free-stream vortices. *J. Fluid Mech.* **764**, R2. doi:10.1017/jfm.2014.731
Singh, K. and Lumley, J. L. (1971). Effect of roughness on the velocity profile of a laminar boundary layer. *Appl. Sci. Res.* **24**, 168-186. doi:10.1007/BF00411712
Squire, L. C. (1961). The motion of a thin oil sheet under the steady boundary layer on a body. *J. Fluid Mech.* **11**, 161-179. doi:10.1017/S0022112061000445
Wainwright, D. K. and Lauder, G. V. (2016). Three-dimensional analysis of scale morphology in bluegill sunfish, lepomis macrochirus. *Zoology* **119**, 182-195. doi:10.1016/j.zool.2016.02.006
Wainwright, D. K. and Lauder, G. V. (2017). *Mucus Matters: The Slippery and Complex Surfaces of Fish*, pp. 223-246. Cham: Springer International Publishing.
Wainwright, D. K., Lauder, G. V. and Weaver, J. C. (2017). Imaging biological surface topography in situ and in vivo. *Methods Ecol. and Evolution* **8**, 1626-1638. doi:10.1111/2041-210X.12778
Wen, L., Weaver, J. C. and Lauder, G. V. (2014). Biomimetic shark skin: design, fabrication and hydrodynamic function. *J. Exp. Biol.* **217**, 1656-1666. doi:10.1242/jeb.097097
Wu, L., Jiao, Z., Song, Y., Liu, C., Wang, H. and Yan, Y. (2018). Experimental investigations on drag-reduction characteristics of bionic surface with water-trapping microstructures of fish scales. *Sci. Rep.* **8**, 12186. doi:10.1038/s41598-018-30490-x
Yanase, K. and Saarenrinne, P. (2015). Unsteady turbulent boundary layers in swimming rainbow trout. *J. Exp. Biol.* **218**, 1373-1385. doi:10.1242/jeb.108043